Removal and recovery of SO_2 and NO in oxy-fuel combustion flue gas by calcium-based slurry

Yuyang Cai[1,2], Xiaohan Ding[3], Wei Li[1,2,4], Dunyu Liu[1,2,], Jun Chen[1,2,*], Mingguo Ni[1,2], Kailong Xu[1,2], and Jing Jin[1,2]*

[1]School of Energy and Power Engineering, University of Shanghai for Science and Technology, 200093 Shanghai, China
[2]Shanghai Key Laboratory of Multiphase Flow and Heat Transfer in Power Engineering, University of Shanghai for Science and Technology, 200093 Shanghai, China
[3]Department of Computer Science, George Mason University, Commonwealth of Virginia, USA
[4]DONGFANG TURBINE Co.,LTD, 618000 Deyang, China

Abstract. This study investigates the use of calcium-based slurry for simultaneous removal NO and SO_2 from oxy-fuel combustion flue gas, and recovery of the sulfur and nitrogen species in resulting solutions. The experiments were performed in a bubbling reactor in a transient mode under the pressure of 20 bar. The various influencing factors including the CaO amount, carrier gas (N_2/CO_2), and absorption time on the simultaneous NO and SO_2 removal process, and the solution products were studied comprehensively. The results show that the NO_2 removal efficiency can be improved by the presence of CO_2, and the gas phase HNO_2 produces in this process. The addition of CaO has positive effects not only on the NO_2 removal efficiency but also on the formation of stable HNO_3. With the presence of CO_2, $CaCO_3$ is formed in a solution initially. With the decrease of pH, $CaCO_3$ is gradually converted to $CaSO_4$, and in particular $CaCO_3$ can be fully avoided through decreasing the pH of an absorption solution to 1.14. At the same time, the formation of unstable S(IV) and NO_2^- can be prevented when the solution pH is lower than 1.37. The nitrogen and sulfur compounds in the absorption solution (at pH 1.14) were further separated by the addition of different amounts of CaO. In particular, 95% of SO_4^{2-} finally can be recovered in the form of $CaSO_4 \cdot 2H_2O$ with nitrogen in solution existing as NO_3^- by controlling the Ca/S ratio at 4.70. The effectiveness of calcium-based slurry on the removal and recovery of SO_2 and NO is confirmed.

1 Introduction

In order to reduce the greenhouse gas CO_2 emission, various pre-combustion, post-combustion (e.g., carbon capture and storage, CCS) and combustion enhanced (e.g., oxy-fuel combustion) technologies have been proposed[1]. Oxy-fuel combustion technology is considered to be one of the most promising ways for carbon capture[2]. This technology not only effectively enriches flue gas with high CO_2 concentration[3], but also effectively reduces NO and SO_2 emissions per unit mass of fuel[4]. However, the NO and SO_2 concentrations are higher in the oxy-fuel combustion flue gas than those in conventional air-combustion flue gas[5]. Therefore, these acid gases (mainly includes NO and SO_2) must be removed from CO_2 stream considering the safety of transport pipelines and sequestration sites.

Currently, the techniques used in existing power plants to remove SO_2 and NO are often independent. The selective catalytic reduction (SCR) and selective noncatalytic reduction (SNCR) technologies are adopted for NO removal[6], while the wet flue gas desulfurization (WFGD) technology using calcium based solution is adopted for SO_2 removal[7]. In the flue gas, NO accounts for more than 90% of the NO_x[8], and is insoluble in aqueous solution. Thereupon, oxidizing insoluble NO to soluble NO_2 before wet scrubbing method is necessary. In this oxidizing process, many oxidation-absorption combined processes have been studied extensively to oxidize NO to NO_2 for the purpose of simultaneous removal of NO and SO_2, including strong oxidizing agent injection[9], selective catalytic oxidation[10,11], and photo-catalytic oxidation[12].

Apart from conventional technologies for NO and SO_2 removal, many new approaches have been proposed specifically for cleaning oxy-fuel combustion flue gases, mainly including two-stage and one-stage methods. Air Products proposed a two-stage scrubbing process with the low pressure (1.5 MPa) and high pressure (3 MPa) stage to remove SO_2 and NO separately in the forms of H_2SO_4 and HNO_3[13]. Similarly, Linde also proposed a two-stage method with the first stage (atmospheric pressure) to remove SO_2 as $CaSO_4$, and second stage (1.8 MPa) to remove NO as NH_4NO_3[14]. In addition, Air Liquide proposed using a sodium solution to remove SO_2 in the atmospheric caustic scrubber, and using a four-stage compression process (at a final pressure of 2.4 MPa) to remove NO in the condensates in the form of HNO_3[15]. Previous methods generally use the two-stage method for

*Corresponding author: Dunyu Liu; Email address: liudunyu@usst.edu.cn; Jun Chen; Email address: j.chen@usst.edu.cn

the removal of SO_2 and NO separately, and this method increases the infrastructure cost, while using the one-stage method to remove both SO_2 and NO is limited. Although the costs for infrastructure and operation for the one stage scrubbing method are significantly reduced, the products are generally mixed in compounds containing sulfur and nitrogen[16], which is detrimental for recovering the sulfur and nitrogen compounds.

Currently, the one-stage method utilizing water solvents to remove both SO_2 and NO at a high pressure is extensively studied[17-20]. These studies have reached the following consensus: (1) the liquid products mainly include H_2SO_4, HNO_3, H_2SO_3, and HNO_2 in this process[18]; (2) this process is heavily dependent upon the pH level[19]; (3) the reaction between HNO_2 and H_2SO_3 is critical for the absorption rates of NO_x and SO_x from the gas to the liquid phase[20]. Moreover, the modeling study mentioned that gas phase HNO_2 (HONO) can be produced in this process[20], but it is not identified in the experimental process[21]. Since Platt et al.[22] first measured the HNO_2 concentration in the atmosphere by differential absorption spectroscopy (DOAS), the importance of HNO_2 in atmospheric chemistry has gradually become known. At the same time, the modeling method can easily obtain the dynamic changes of unstable H_2SO_3 and HNO_2 in solution[23], but these products have not been systematically studied through experiments. Therefore, the quantification of the gas phase HNO_2, the liquid phase H_2SO_3, and HNO_2 is critical for the understanding the simultaneous absorption of SO_2 and NO and implementing simultaneous removal technique in the practical applications.

In this work, the one-stage method utilizing calcium-based slurry was adopted to remove NO and SO_2 in the oxy-fuel combustion flue gas, and also to recover the sulfur and nitrogen compounds in the forms of $CaSO_4{\cdot}2H_2O$ precipitate and NO_3^-. This approach can potentially reduce the operation cost through the utilization of the low-cost absorbents and the recovery of the end products. The effects of the CaO amount and absorption time on the removal efficiency of SO_2 and NO as well as the effectiveness of the recovery of H_2SO_4 and HNO_3 are discussed. In addition, the mechanisms for simultaneous removal, and recovery processes are elucidated.

2 Experimental methods

2.1 Experimental apparatus and method

As shown in Fig.1, the experimental apparatus mainly included a high pressure bubbling reactor, four high pressure mass flow controllers, a light source, an optical lens, an absorption cell, a spectrograph and an MRU delta 2000 flue gas analyzer. The high pressure mass flow controllers were used to control the flow rate of the simulated flue gas into the high pressure bubbling reactor, including O_2 (purity > 99.999%), N_2/CO_2 (purity > 99.999%), 1% (NO in N_2) and 3% (SO_2 in N_2). The 316 stainless steel tube was used as the gas transmission line, and the total flow rate of the simulated flue gas was 2 L/min. The simulated flue gas was introduced to the cylinder reactor from top of the reactor to nearly the bottom of the reactor through a 1/8 inch tube to maximize the residence time of gas mixture in the reactor. The volume of the reactor was 1 L with half-filled with absorption solution. The average residence time was obtained by dividing the volume of reactor by the gas flow rate. Under the pressure of 20 bar, the residence time of gas mixture in liquid phase is 300 s. During the contact between gas and liquid, soluble gases in the gas mixture were absorbed into absorption solution. Above the absorption solution, gases containing water vapor flowed upwards to the outlet of the cylinder reactor. The pressure inside the reactor was controlled by the pressure regulator. Following the regulator, the simulated flue gas flowed to the absorption cell, where the NO_2 and HNO_2 concentrations were measured online by the DOAS. After the absorption cell, the simulated flue gas was partially drawn to the MRU delta 2000 flue gas analyzer for the measurement of the SO_2, NO, and O_2 concentrations, and the residual flue gas was washed before being vented to atmosphere.

The operation procedures are given as follows. 0.5 L of deionized water with a certain amount of CaO was first introduced into the reactor. The bypass valve was turned on, and then the concentrations of O_2, N_2/CO_2, NO, and SO_2 were set to the required concentrations. After 10 minutes stabilization, all the gas bottles were turned off and N_2/CO_2 gas bottle was left to rinse the gases of NO and SO_2 in the system. After that, the bypass valve was turned off, and the N_2/CO_2 gas was continuously introduced into the reactor to pressurize the reactor to the set pressure, and then the simulated flue gas was continuously introduced into the reactor. In all experiments, the inlet concentrations of O_2, N_2/CO_2, NO, and SO_2 were set at 5%, 75%/75%, 1000 ppm, and 2000 ppm, respectively, and the pressure selected was 20 bar. In addition, the pH of the absorption solutions after experiments was determined by a pH meter. The concentrations of SO_4^{2-} and NO_3^- in solution were measured by the UV–visible spectrophotometry[24], while the concentrations of S(IV) (i.e., HSO_3^-, SO_3^{2-}, and SO_2) and NO_2^- in solution were determined by the acid desorption method. The solid by-products of the absorption solutions were identified by the X-ray diffraction (XRD-6100). Above measurements were sampled after the experiment.

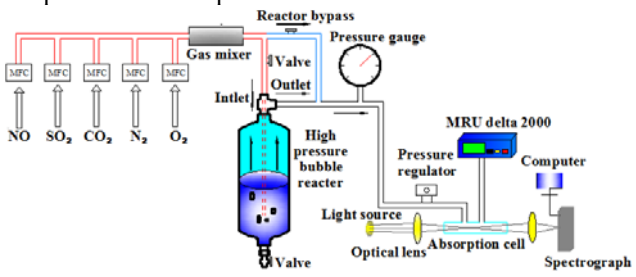

Fig. 1. The schematic diagram of experimental apparatus

2.2 Measurement methods

2.2.1 Measurement of the gas phase NO, NO_2,

HNO_2, and SO_2

The MRU delta 2000 flue gas analyzer was used to measure the SO_2 and NO concentrations, whereas the NO_2 and HNO_2 concentrations were measured online by the DOAS. The absorption characteristics of different gases are different in spectral bands because of the different structures of gas molecules. The measurement of different gases by the DOAS utilized the selective absorption of light from the ultraviolet to near-ultraviolet bands by gases. When a light source with an incident light intensity of I_0 passes the measuring medium, and then the emitted light intensity is I due to the radiation absorption of different gases. The Lambert Beer's law expressed by Eq. (1) describes the relationship between I and I_0.

$$\alpha = \frac{\ln\left(\frac{I_0}{I}\right)}{L} = \sum_i^n C_i \sigma_i \tag{1}$$

where α is the absorption coefficient; I_0 and I are the incident and emitted light intensity, respectively, candela; σ_i is the absorption cross section, m^2; L is the absorption cell length, 0.35 m; C_i is gas concentration, ppm. NO_2 absorbs the lights with the spectral range from 340 nm to 400 nm[25]. The near-ultraviolet absorption peak of HNO_2 is 341.8 nm, 354.2 nm, and 368 nm, respectively[26]. The center wavelength of the light source used in the experiment was 355 nm, and the full width at half the maximum light intensity was 15 nm. Therefore, in the spectral range from 340 nm to 370 nm, the least-squares fitting method was adopted for the calculations of the HNO_2 and NO_2 concentrations. Fig.2 shows the spectral fitting results for a single-point simultaneous measurement of both the NO_2 and HNO_2[27]. By comparing the magnitudes of the absorption coefficients for fitting results with these for residuals, the absorption coefficients for NO_2 is two magnitudes higher than residuals while the absorption coefficients for HNO_2 is the same magnitude with the residuals. Therefore, the measurement for NO_2 may be more accurate than the measurement for HNO_2.

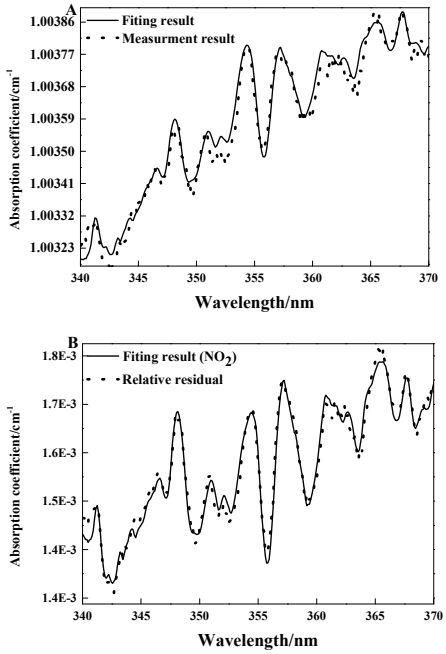

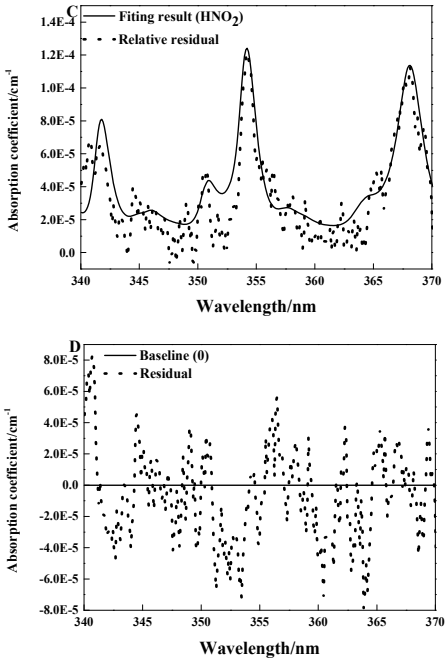

Fig. 2. Spectral fitting results for a single-point simultaneous measurement of both NO_2 and HNO_2. (A) measurement and fitting results in the spectral range from 340 nm to 370 nm; (B) spectral fitting results for NO_2; (C) spectral fitting results for HNO_2; (D) residuals after spectral fitting

2.2.2 Measurement of the liquid phase NO_3^-, SO_4^{2-}, S(IV), and NO_2^-

The concentrations of NO_3^- and SO_4^{2-} in solution were measured by UV–visible spectrophotometry, which used the specific wavelength to measure the corresponding substance. Before the measurement, the standard curve for the standard solutions versus the corresponding absorbance was obtained by experiments. The substance concentrations at different absorbance could be regressed from the standard curve. When the light source passes through the solution to be tested, the absorbance of the solution is proportional to the concentration of the substance in the solution. The relationship is expressed by Eq. (2).

$$A = -\lg\left(\frac{I}{I_0}\right) = KLC \tag{2}$$

where A is the absorbance of the absorption solution; I and I_0 are the incident and emitted light intensity, respectively, candela; K is the molar absorption coefficient; L is the length of the cuvette, 50 mm; C is the concentration of the substance, mol/L.

Based on the above principle, the NO_3^- concentration was measured at the specific wavelength of 220 nm. The SO_4^{2-} concentration was measured by the UV-visible-method of barium-chromate ($BaCrO_4$). Under acidic conditions, the reaction between $BaCrO_4$ and SO_4^{2-} forms $BaSO_4$ precipitates and the CrO_4^{2-} ions which have the maximum absorption at 420 nm. After filtering the $BaSO_4$ precipitates, the CrO_4^{2-} concentration could be obtained

by measuring the absorbance of the solution, so the SO_4^{2-} concentration can be obtained because the CrO_4^{2-} concentration is equal to the SO_4^{2-} concentration.

The S(IV) and NO_2^- concentrations in solution were measured by acid-promoted desorption method. In order to completely convert S(IV) to SO_2, a certain amount of HCl (1 ml 2.5 mol/L HCl) was added to the absorption solution (5 mL), and then the absorption solution was purged with 2 L/min of N_2 with the discharged gas measured by the MRU delta 2000 flue gas analyzer for the SO_2 concentration. When the SO_2 concentration was zero, the N_2 purging process was terminated. The total S(IV) concentration in a solution was calculated by integrating the SO_2 concentration against time within the desorption period. In order to verify the accuracy of this method, the standard $NaHSO_3$ solutions with four concentrations of 0.0025, 0.005, 0.01, and 0.02 mol/L were measured with relative errors for these measurements being less than 3%.

Similarly, the NO_2^- concentration in solution was also measured by acid-promoted desorption. After adding a certain amount of HCl (1 ml 2.5 mol/L HCl), NO_2^- was converted to HNO_2 which could be desorbed in the forms of NO, NO_2, and HNO_2. Four standard $NaNO_2$ solutions (0.0025, 0.005, 0.01, and 0.02 mol/L) were used to validate the accuracy of NO_2^- measurement. Overall, the accuracy of acid-promoted desorption method was over 90%.

3 Results and discussion

3.1 Effects of CaO amounts on the simultaneous NO and SO_2 removal process

To investigate the influence of CaO amounts on the NO and SO_2 removal process, different amounts of CaO (0, 0.285, 0.570, and 0.855 g) were introduced into water to make up a total liquid volume of 0.5 L. The experiments were performed in the presence or absence of CO_2 at room temperature. As shown in Figs. 3-A, 3-A', 3-B, and 3-B', the concentrations of NO and NO_2 at the outlet of bubble reactor gradually increased with time. Both of them increased significantly initially within 10 min, and then increased slowly after that. The initial 10 min quick increase for both NO and NO_2 could be due to the retention time of the bubble reactor before the gas analyzer.

The slow increase of NO and NO_2 after the quick initial increase may come from the complex chemical reactions between the gas phase NO and NO_2 with water. NO is considered oxidized easily under high pressure to form NO_2[28]. Through forming high soluble intermediate, the absorption of NO and NO_2 into water is greatly enhanced to form HNO_2, and HNO_3[29]. HNO_3 is quite stable in solution, while HNO_2 is easily decomposed to form HNO_3 and NO at room temperature[30]. The different proportions of HNO_2 and HNO_3 is strongly dependent on the solution pH[31]. The decomposition of HNO_2 to HNO_3 and NO was enhanced with the decrease of the liquid pH, which results in the increase of NO in the gas phase. In a similar way, this also results in increasing NO_2 in the gas phase due to the re-oxidation of NO to NO_2[31].

By comparing with the case in the presence of CaO, it can be seen that the introduction of CaO into water markedly enhanced NO and NO_2 absorption. NO and NO_2 absorption increased with the increase in the amount of CaO. The reason for this result is that the CaO dissolves into water to increase the alkalinity of the solution, and the alkaline condition leads to slightly higher NO and NO_2 absorption efficiencies[32]. Furthermore, the NO_2 absorption is further promoted when CO_2 is present in the gas phase. This can be explained that in the presence of CO_2, the Ca^{2+} preferentially participates in the formation of $CaCO_3$; in the absence of CO_2, the Ca^{2+} preferentially participates in the formation of low solubility $CaSO_3$, which is detrimental for the NO_2 absorption[33].

Figs. 3-C and 3-C' show that the outlet of HNO_2 concentration increased slightly over time, and the HNO_2 concentration was approximately 5 ppm. Both the presence of CO_2 and the addition of CaO had little effect on the production of HNO_2. SO_2 was not observed at the outlet of bubble reactor for all the experiments indicating that all SO_2 can be absorbed because of the instantaneous reaction of SO_2 with water[30].

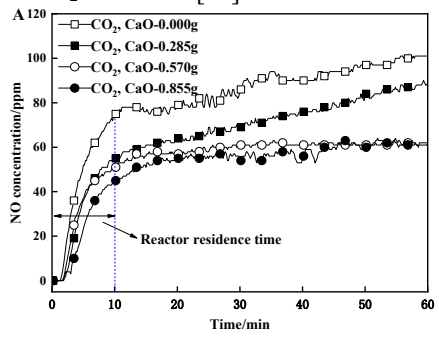

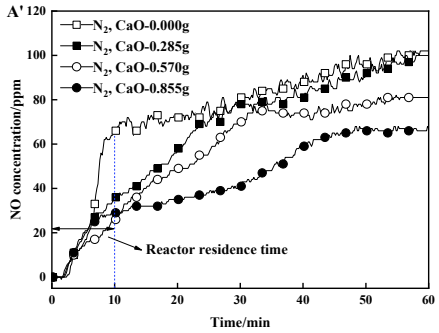

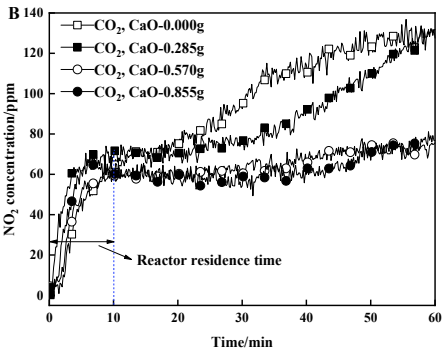

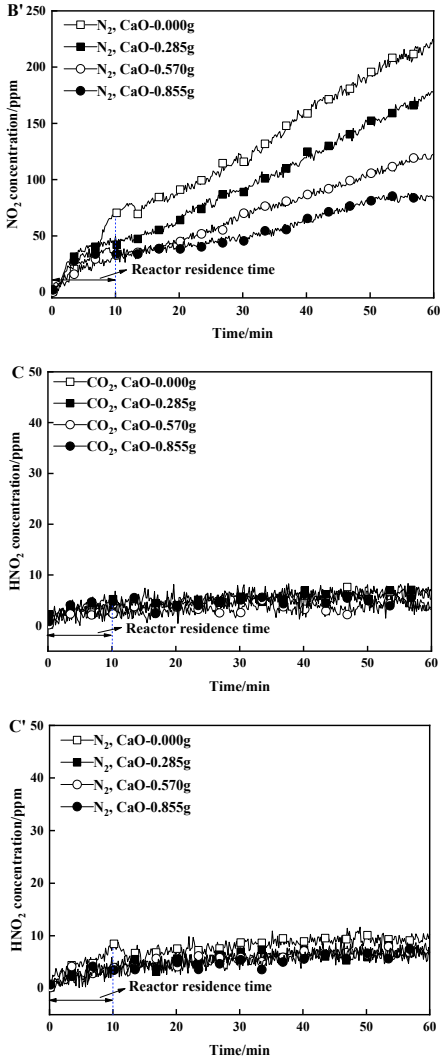

Fig. 3. The comparison on the gas outlet concentrations of NO ((A) and (A')), NO_2 ((B) and (B')) and HNO_2 ((C) and (C')) in the presence or absence of CO_2 (inlet NO concentration is 1000 ppm, CO_2 and N_2 stand for CO_2 and N_2 atmosphere, respectively)

The dynamic changes of the concentrations of SO_4^{2-}, NO_3^-, S(IV), NO_2^-, and the solution pH are shown in Fig.4. As shown in Fig.4, CO_2 has a slight effect on the NO_3^-, S(IV), NO_2^- concentrations, and remarkable effect on the SO_4^{2-} concentration, the solution pH. Both the SO_4^{2-} and NO_3^- concentrations increased with time, and NO_3^- concentrations were quite similar. However, in the presence of CO_2, the SO_4^{2-} concentration was much higher than that in the absence of CO_2, and this is caused by the reaction between SO_4^{2-} and Ca^{2+} to form $CaSO_4$ precipitate to consume SO_4^{2-}[33], while in the presence of CO_2, the Ca^{2+} exists in solution in the form of $CaCO_3$. In the presence of CO_2, the solution pH initially dropped more slowly compared with that in the absence of CO_2. Because the formed $Ca(OH)_2$ can be rapidly consumed by HCO_3^- to form $CaCO_3$ in the pressurization process. However, in the presence of CO_2, the final pH (pH = 2.79) (60 min) was much higher than that (pH = 1.92) (60 min) in the absence of CO_2, and this may be caused by the formed $CaCO_3$, which may work as a buffer in liquid. Meanwhile, both the S(IV) and NO_2^- concentrations first increased, and then decreased dramatically with time because strong acidic conditions accelerate the decomposition of both the S(IV) and NO_2^-[34], so that their concentrations (60 min) became very low.

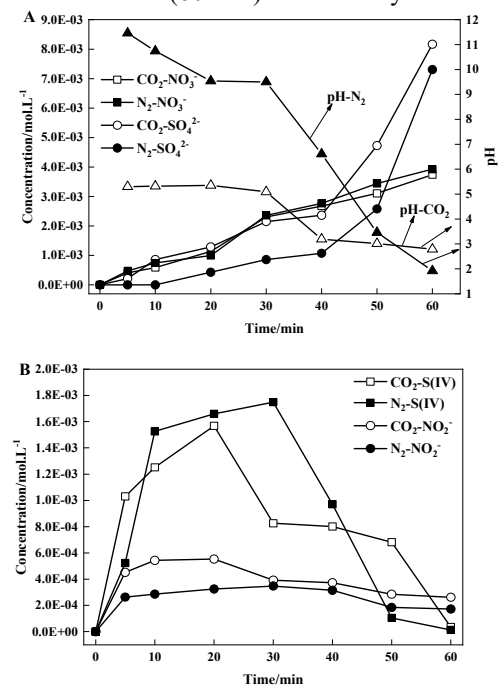

Fig. 4. Dynamic changes of the solution pH (A), the concentrations of SO_4^{2-} (A), NO_3^- (A), S(IV) (B), and NO_2^- (B) with 0.570 g CaO addition into water

The concentrations of SO_4^{2-}, NO_3^-, and the solution pH under different amounts of CaO (0, 0.285, 0.570, and 0.855g) introduced into water for the absorption time of 1 h are shown in Fig.5. From Fig.5, one finds that CaO has a remarkable effect on the NO_3^-, S(IV), NO_2^-, SO_4^{2-} concentrations, and the solution pH. With the increase of CaO, the final solution pH increased as well, and this can be interpreted that the reaction between CaO and H_2O forms alkaline $Ca(OH)_2$ which increases the alkalinity of solutions. The NO_3^- concentration increased with the increase of CaO, and in contrast, the SO_4^{2-} concentration decreased with the increase of CaO. This may be due to the formation of insoluble $CaSO_4$ by the reaction between SO_4^{2-} and Ca^{2+}. The concentrations of S(IV) and NO_2^- decreased with the increase of CaO. Overall, the introduction of CaO into water is more favorable for the formation of stable $CaSO_4$ precipitates and NO_3^-.

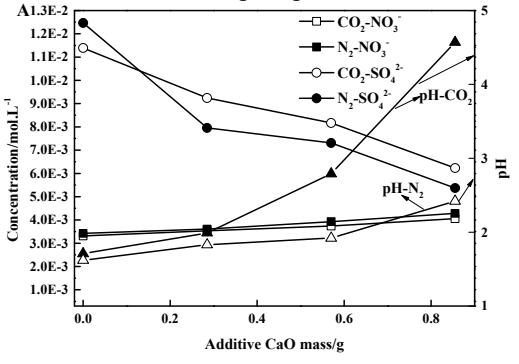

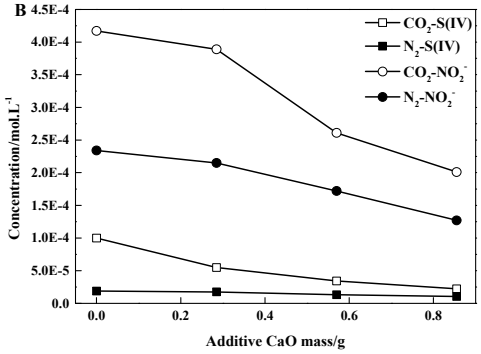

Fig. 5. The final pH (A), the concentrations of SO_4^{2-} (A), NO_3^- (A), S(IV) (B) and NO_2^- (B) under different additions of CaO into water at an absorption time of 1h

XRD analysis was used to determine the crystal composition of precipitate after gas absorption. Both dried and wet precipitates were analyzed. In the presence of CO_2, the only precipitate was $CaCO_3$, whereas in the absence of CO_2, the only precipitate was $CaSO_4{\cdot}2H_2O$. In comparison, the most popular WFGD uses $CaCO_3$/CaO to remove SO_2 and NO, and the by-product of this process mainly includes $CaSO_3$[35,36]. The comparison indicates that in a high pressure scrubbing process, the generated $CaSO_3$ can be oxidized to $CaSO_4$ by dissolved NO_2 and O_2 effectively[37,38], and $CaSO_4$ further reacts with H_2O to form $CaSO_4{\cdot}2H_2O$[37]. From the aspect of economy, the byproduct $CaSO_4{\cdot}2H_2O$ has a higher recycling value than $CaSO_3$. The utilization of by-product $CaSO_4{\cdot}2H_2O$ can reduce the operation cost of a scrubber.

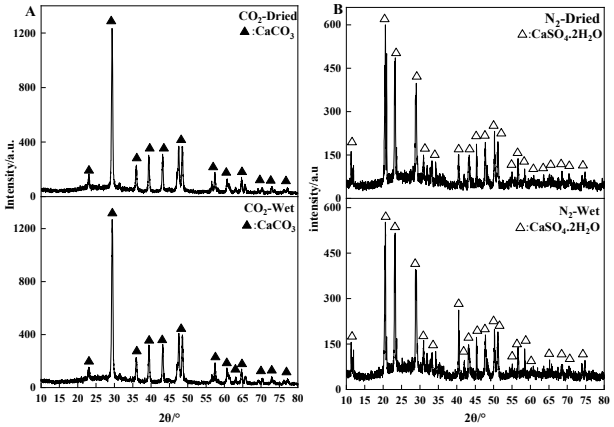

Fig. 6. XRD patterns of the precipitate at gas absorption of 1 h with 0.885 g CaO addition into water. (A) CO_2 atmosphere; (B) N_2 atmosphere

As CO_2 is dominate in the gas phase for oxy-fuel combustion flue gas, the formation of $CaCO_3$ cannot be avoided. However, $CaCO_3$ is reactive towards SO_2[39,40], and therefore, $CaCO_3$ can be converted to $CaSO_4$ if enough reaction time is provided.

3.2 Effects of absorption time on the simultaneous NO and SO_2 removal process

The absorption time was prolonged to avoid the calcium exist in the form of $CaCO_3$. The experiments were carried out under the same amount of CaO (0.855g) in the presence of CO_2 with different absorption times including 5, 10, 20, 40, 60, 180, and 240 min. Fig.7 shows the dynamic changes of the concentrations of SO_4^{2-}, NO_3^-, S(IV), NO_2^-, and the solution pH. Based on Fig. 7-A, the solution pH had a slight increase (from pH 4.78 to pH 5.66) within 20 min, and this result may be due to the addition of excessive CaO. In this pH range, the S(IV), NO_2^-, and NO_3^- began to form, and in particular, both the S(IV) and NO_2^- concentrations reached the maximum at a pH 5.66. From pH 5.66 to pH 1.37, both the concentrations of S(IV) and NO_2^- sharply decreased to zero, while both the SO_4^{2-} and NO_3^- were increasingly formed with time. In this pH range, following two processes may occur: (1) some S(IV) (mainly includes SO_3^{2-} and HSO_3^-) are gradually oxidized into SO_4^{2-} by the dissolved NO_2 and O_2[41,42]; (2) some S(IV) react with Ca^{2+}/$CaCO_3$ to form $CaSO_3$. With the decrease of solution pH, NO_2^- is gradually converted to HNO_2 which is more easily decomposed to HNO_3 and NO, and this result in the NO_2^- decreasing to zero. From pH 1.37 to pH 1.14, both the SO_4^{2-} and NO_3^- concentrations reached the maximum because the continuous absorption of SO_2 and NO*x* into water to form the SO_4^{2-} and NO_3^-.

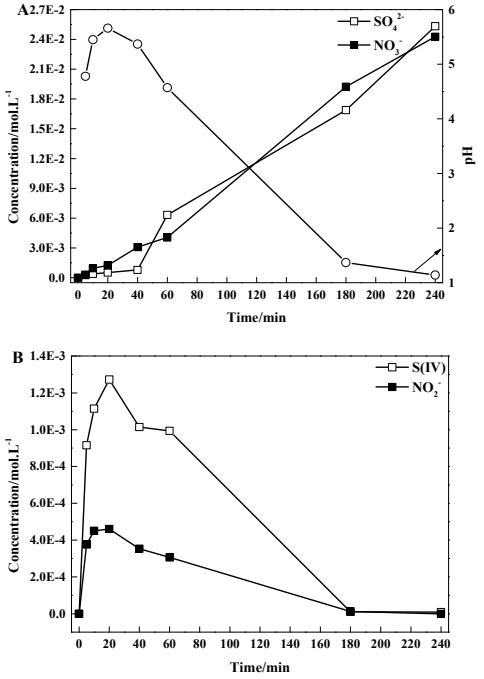

Fig. 7. Dynamic changes of the solution pH (A) and the concentrations of SO_4^{2-} (A), NO_3^- (A), S(IV) (B), and NO_2^- (B)

The XRD patterns of the precipitate of the absorption solution are shown in Fig.8. From 5 min (pH = 4.78) to 60 min (pH = 4.57), the only precipitate was $CaCO_3$. When the absorption time was increased to 180 min (pH = 1.37), the precipitate included $CaCO_3$ and $CaSO_4{\cdot}2H_2O$. Furthermore, when the absorption time was increased to 240 min (pH = 1.14), the only precipitate was $CaSO_4{\cdot}2H_2O$. Above results indicate that when solution pH was above 4.57, the formed $CaCO_3$ can stably exist, but when the pH was reduced to 1.14, the formed $CaCO_3$ can be completely decomposed by the formed H_2SO_3, HNO_3, and H_2SO_4. At the same time, the formed sparingly soluble $CaSO_3$ can be oxidized to $CaSO_4$ by the dissolved

NO_2 and O_2[37,38]. The reaction between $CaSO_4$ and H_2O also takes place in this process. In practical situation, the controllable factor is the pH of the solution. Above results indicate that $CaCO_3$ can be avoided through decreasing the pH of absorption solution to 1.14.

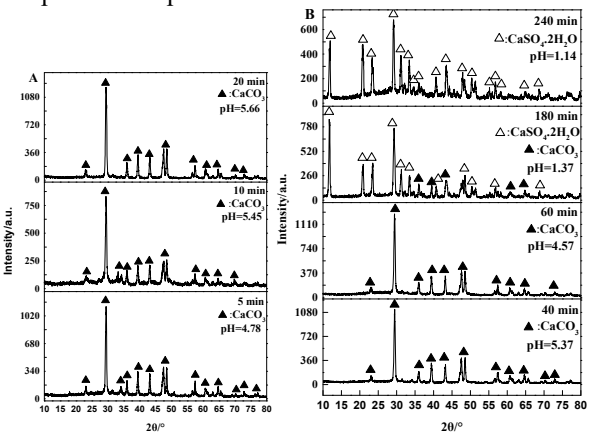

Fig. 8. XRD patterns of the precipitates for seven absorption times including 5min (A), 10 min (A), 20 min (A), 40 min (B), 60 min (B),180 min (B), and 240 min (B)

3.3 Effects of the ratios of Ca/S on the recovery process

As can be seen from Fig.7-A, the obtained absorption solution still contained a considerable amount of SO_4^{2-} (2.53×10^{-2} mol/L) and NO_3^- (2.43×10^{-2} mol/L) at the absorption time of 240 min indicating the absorption process cannot effectively separate SO_4^{2-} and NO_3^- for further utilization. To further separate SO_4^{2-} and NO_3^- in the solutions, a simple approach was to add more CaO into the solution to promote further conversion of SO_4^{2-} to $CaSO_4$ precipitate. An optimum ratio of Ca/S may exist for separating SO_4^{2-} and NO_3^- from the solution. Different amounts of CaO (0, 1.07×10^{-4}, 3.57×10^{-4}, and 5.35×10^{-4} mol) were added to a 3 mL of the solution (7.59×10^{-5} mol SO_4^{2-}), and then stored at atmospheric temperature and pressure for 24 h. The corresponding ratios of Ca/S are 0, 1.41, 4.70, and 7.05, respectively.

Figs.9-A, and 9-B show the SO_4^{2-} concentration decreased sharply with the increase in the ratio of Ca/S. In this process, SO_4^{2-} in solution was converted to $CaSO_4 \cdot 2H_2O$ precipitate. It can be expected that the higher Ca/S ratio is more favorable for the conversion of SO_4^{2-} to $CaSO_4 \cdot 2H_2O$ precipitate, while the NO_3^- concentration stays at the same value as the initial concentration. Through controlling the Ca/S ratio at 4.70, the only precipitate was $CaSO_4 \cdot 2H_2O$, and there still existed 5% SO_4^{2-} in the solution. Moreover, increasing the Ca/S ratio to 7.05 can promote the conversion of 98% SO_4^{2-} to $CaSO_4 \cdot 2H_2O$ precipitate, but the precipitates contained $CaSO_4 \cdot 2H_2O$ and $Ca(OH)_2$. From the above-mentioned analysis, the optimum ratio of Ca/S is 4.70, and the corresponding pH is 8.94.

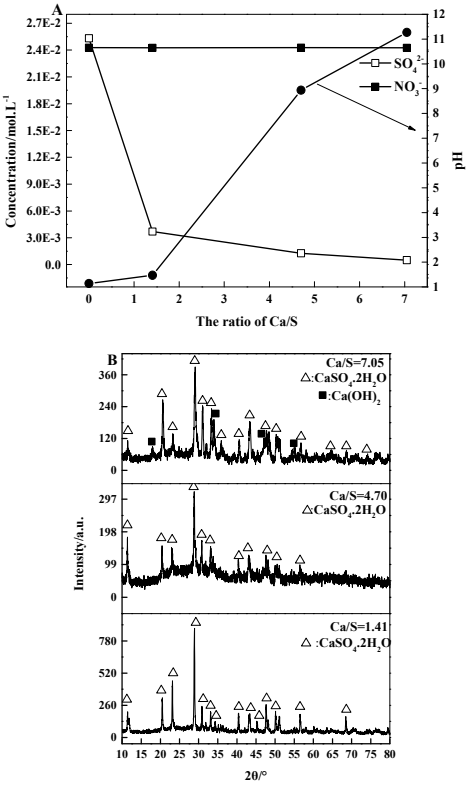

Fig. 9. Dynamic changes of the pH (A), the concentrations SO_4^{2-} (A), NO_3^- (A) and the XRD patterns of the precipitates (B) under different ratios of Ca/S

3.4 Proposing the mechanism for simultaneous removal and recovery of NO and SO_2

The schematic diagram of the reaction pathway for simultaneous removal, and recovery of NO and SO_2 including the pressurization, absorption, and recovery processes is shown in Fig.10. The solution pH has a significant effect on the products formation. In the pressurization process, CaO firstly reacts with H_2O to form $Ca(OH)_2$ (R1), and then it is rapidly consumed by HCO_3^- to form $CaCO_3$ precipitate (R2, R3).

Compared to the pressurization process, the absorption process is more complicated. With the introduction of the simulated flue gas, NO can be converted into NO_2 by O_2 under high pressure (20 bar) in the gas phase (R4)[20]. NO and NO_2 may also react with water vapor to form the gas phase HNO_2 (R5)[43]. In the liquid phase absorption process, from pH 4.78 to pH 5.66, the NO_2^-, NO_3^- and S(IV) begin to form due to the hydrolysis of SO_2 and NO_2 (R6–R9)[31]. However, some S(IV) (mainly includes SO_3^{2-} and HSO_3^-) can be oxidized into the SO_4^{2-} by NO_2 and O_2 (R10, R11)[41,42], and some S(IV) react with $Ca^{2+}/CaCO_3$ (R12, R15) to form $CaSO_3$ which can be oxidized to $CaSO_4$ by the dissolved NO_2 and O_2 (R16, R17)[37,38], and with the decrease of solution pH, NO_2^- is gradually converted to HNO_2 which is more easily decomposed to HNO_3 and NO (R18). From pH 5.66 to pH 1.37, both the NO_2^- and S(IV) concentrations decrease to zero, whereas both the NO_3^- and SO_4^{2-} increasingly form,

and the formed $CaCO_3$ is gradually decomposed to form $CaSO_4.2H_2O$ (R12–R14). From pH 1.37 to pH 1.14, the residual formed $CaCO_3$ can be completely decomposed to form $CaSO_4.2H_2O$ by the formed HNO_3 and H_2SO_4. In this pH range, following two processes occur: (1) the residual formed Ca^{2+} reacts with SO_4^{2-} to $CaSO_4$ (R19); (2) the formed $CaSO_4$ reacts with H_2O to form $CaSO_4.2H_2O$ (R20).

In the separation process, the absorption solution (at a pH of 1.14) only contains H_2SO_4 and HNO_3, and CaO was introduced into the obtained absorption solution to further separate H_2SO_4 and HNO_3. When the ratio of Ca/S is 4.70, the solution pH is 8.94, and these reactions only take place in solution to form $CaSO_4{\cdot}2H_2O$ and Ca^{2+}, NO_3^- (R19–R22). When the ratio of Ca/S is 7.05, the solution pH is 11.27. As excess CaO is added to the solution, and CaO cannot be fully consumed by H_2SO_4 and HNO_3. Reactions take place in solution to form $Ca(OH)_2$, $CaSO_4{\cdot}2H_2O$, and Ca^{2+}, NO_3^- (R1, R19–R22).

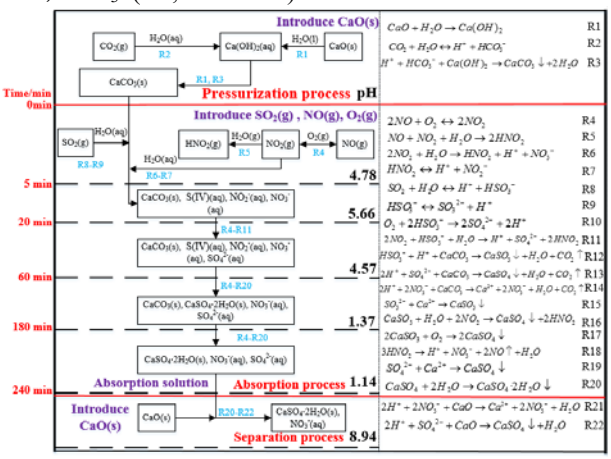

Fig. 10. Schematic diagram of the proposed reaction pathways for simultaneous removal and separation of SO_2 and NO against time

4 Conclusions

Wet-based method using calcium-based slurry was proposed for simultaneous removal of SO_2 and NO from oxy-fuel combustion flue gas at a high pressure while recovering products as the $CaSO_4{\cdot}2H_2O$ precipitate and NO_3^-. This process was developed and investigated through experiments. The following conclusions can be drawn:

(1) NO is effectively oxidized to NO_2 at a pressure of 20 bar, and the gas phase HNO_2 is produced in this process. The presence of CO_2 in the simulated flue gas can enhance the NO_2 absorption. At the same time, the addition of CaO into water not only enhances the NO_2 absorption but also the formation of HNO_3.

(2) In the presence of CO_2 in the simulated flue gas, the initial formed $CaCO_3$ can be completely converted into $CaSO_4{\cdot}2H_2O$ through decreasing the pH of absorption solution to the pH 1.14. Both the formation of S(IV) and NO_2^- can be prevented when the solution pH is lower than 1.37.

(3) As high as 95% SO_4^{2-} in the obtained absorption solution can be recovered in the form of $CaSO_4{\cdot}2H_2O$ by controlling the ratio of Ca/S at 4.70.

Acknowledgement

This research was funded by National Natural Science Foundation of China (project Nos. 51706143 and 51976129), supported by the Shanghai Pujiang Program (16PJ1407900).

References

1. Kanniche M, Gros-Bonnivard R, Jaud P, Valle-Marcos J, Amann JM, Bouallou C. Pre-combustion, post-combustion and oxy-combustion in thermal power plant for CO_2 capture. *Appl. Therm. Eng*. **30** (2010): 53-62.
2. Krzywanski J, Czakiert T, Muskala W, Nowak W. Modelling of CO_2, CO, SO_2, O_2 and NO*x* emissions from the oxy-fuel combustion in a circulating fluidized bed. *Fuel Process. Technol*. **92** (2011): 590-596.
3. Luo Z, Cheng W, Wu B, Zhao Y, Zhang J. A mode transition strategy from air to oxyfuel combustion in a 35 MW coal-fired power plant boiler. *Korean J. Chem. Eng*. **34** (2017): 1554-1562.
4. Fleig D, Andersson K, Johnsson F, Leckner B. Conversion of sulfur during pulverized oxy-coal combustion. *Energ. Fuel*. **25** (2011): 647-655.
5. Yoshiie R, Hikosaka N, Nunome Y, Ueki Y, Naruse I. Effects of flue gas re-circulation and nitrogen contents in coal on NO*x* emissions under oxy-fuel coal combustion. *Fuel Process. Technol*. **136** (2015): 106-111.
6. Tao W, Zhang X, Liu J, Liu H, Guo Y, Sun B. Plasma-assisted catalytic conversion of NO over Cu-Fe catalysts supported on ZSM-5 and carbon nanotubes at low temperature. *Fuel Process. Technol*. **178** (2018): 53-61.
7. Zhu Z, Ma Y, Zan Q, Fang L, Zhang W, Yan N. Study on a new wet flue gas desulfurization method based on the bunsen reaction of sulfur-iodine thermochemical cycle. *Fuel*. **195** (2017): 33-37.
8. Wang Z, Zhang Y, Tan Z, Li Q. A wet process for oxidation-absorption of nitric oxide by persulfate/calcium peroxide. *Chem. Eng. J*. **350** (2018): 767-775.
9. Raghunath CV, Mondal MK. Reactive absorption of NO and SO_2 into aqueous NaClO in a counter-current spray column. *Asia-Pac J Chem. Eng*. **11** (2016): 88-97.
10. Zhao Y, Han Y, Wang T, Sun Z, Fang C. Simultaneous removal of SO_2 and NO from flue gas using iron-containing polyoxometalates as heterogeneous catalyst in UV-Fenton-like process. *Fuel*. **250** (2019): 42-51.
11. Han J, Kim H, Sakaguchi Y, Cheol-Ho K, Yao H. The synergetic effect of plasma and catalyst on

simultaneous removal of SO_2 and NO*x*. *Asia-Pac J Chem. Eng*. **5** (2010): 441-446.

12. Hao L, Hao W, Bao J, Yu X, Yang H. Photochemical removal of NO and SO_2 from flue gas using UV irradiation. *Asia-Pac J Chem. Eng*. **9** (2014): 775-781.
13. White V, Wright A, Tappe S, Yan J. The air products vattenfall oxyfuel CO_2 compression and purification pilot plant at schwarze pumpe. *Energy Procedia*. **37** (2013): 1490-1499.
14. Winkler F, Schoedel N, Zander H-J, Ritter R. Cold deNO*x* development for oxyfuel power plants. *Int. J. Greenh. Gas Con*. **5** (2011): S231-S237.
15. Darde A, Prabhakar R, Tranier J-P, Perrin N. Air separation and flue gas compression and purification units for oxy-coal combustion systems. *Energy Procedia*. **1** (2009): 527-534.
16. Stanger R, Ting T, Spero C, Wall T. Oxyfuel derived CO_2 compression experiments with NO*x*, SO*x* and mercury removal—experiments involving compression of slip-streams from the Callide Oxyfuel Project (COP). *Int. J. Greenh. Gas Con*. **41** (2015): 50-59.
17. Iloeje C O, Field R P, Ghoniem A F, et al. Modeling and parametric analysis of nitrogen and sulfur oxide removal from oxy-combustion flue gas using a single column absorber[J]. Fuel, **160** (2015): 178-188.
18. Ajdari S, Normann F, Andersson K. Evaluation of operating and design parameters of pressurized flue gas systems with integrated removal of NO*x* and SO*x*. *Energ. Fuel*. **33** (2019): 3339-3348.
19. Ajdari S, Normann F, Andersson K, Johnsson F. Reduced mechanism for nitrogen and sulfur chemistry in pressurized flue gas systems. *Ind. Eng. Chem. Res.* **55** (2016): 5514-5525.
20. Ajdari S, Normann F, Andersson K, Johnsson F. Modeling the nitrogen and sulfur chemistry in pressurized flue gas systems. *Ind. Eng. Chem. Res*. **54** (2015): 1216-1227.
21. Ting T, Stanger R, Wall T. Laboratory investigation of high pressure NO oxidation to NO_2 and capture with liquid and gaseous water under oxy-fuel CO_2 compression conditions. *Int. J. Greenh. Gas Con*. **18** (2013): 15-22.
22. Platt U, Perner D, Harris GW, Winer AM, Pitts JN. Observations of nitrous acid in an urban atmosphere by differential optical absorption. *Nature*. **285** (1980): 312-314.
23. Tumsa TZ, Lee SH, Normann F, Andersson K, Ajdari S, Yang W. Concomitant removal of NO*x* and SO*x* from a pressurized oxy-fuel combustion process using a direct contact column. *Chem. Eng. Res. Des*. **131** (2018): 626-634.
24. Cronin AA, Barth JAC, Elliot T, Kalin RM. Recharge velocity and geochemical evolution for the Permo-Triassic Sherwood Sandstone, Northern Ireland. *J. Hydrol*. **315** (2005): 308-324.
25. Voigt S, Orphal J, Burrows JP. The temperature and pressure dependence of the absorption cross-sections of NO_2 in the 250–800 nm region measured by Fourier-transform spectroscopy. *J. Photoch. Photobio. A*. **149** (2002): 1-7.
26. Stutz J, Kim ES, Platt U, Bruno P, Perrino C, Febo A. UV-visible absorption cross section of nitrous acid. *J. Geophys. Res-Atmos*. **105** (2000): 14585-14592.
27. Yu S, Liu D, Chen J. Experimental study on the convesion of NO*x* to nitrous acid at pressres. *Journal of Chinese Society of Power Engineering*. **38** (2018): 725-731(in chinese).
28. Cheng Q, Liu D, Chen J, Jin J, Li W, Yu S. Gas-phase oxidation of NO at high pressure relevant to sour gas compression purification process for oxy-fuel combustion flue gas. *Chinese J. Chem. Eng*. **27** (2019): 884-895.
29. Shen CH, Rochelle GT. Nitrogen dioxide absorption and sulfite oxidation in aqueous sulfite. *Environ. Sci. Technol*. **32** (2015): 1994-2003.
30. Torrente-Murciano L, White V, Petrocelli F, Chadwick D. Study of individual reactions of the sour compression process for the purification of oxyfuel-derived CO_2. *Int. J. Greenh. Gas Con*. **5** (2011): S224-S230.
31. Normann F, Jansson E, Petersson T, Andersson K. Nitrogen and sulphur chemistry in pressurised flue gas systems: a comparison of modelling and experiments. *Int. J. Greenh. Gas Con*. **12** (2013): 26-34.
32. Liémans I, Alban B, Tranier JP, Thomas D. SO*x* and NO*x* absorption based removal into acidic conditions for the flue gas treatment in oxy-fuel combustion. *Energy Procedia*. **4** (2011): 2847-2854.
33. Tang N, Yue L, Wang H, Ling X, Wu Z. Enhanced absorption process of NO_2 in $CaSO_3$ slurry by the addition of $MgSO_4$. *Chem. Eng. J*. **160** (2010): 145-149.
34. Ping F, Cen C, Tang Z, Zhong P, Chen D, Chen Z. Simultaneous removal of SO_2 and NO*x* by wet scrubbing using urea solution. *Chem. Eng. J*. **168** (2011): 52-59.
35. Yi Z, Hao R, Bo Y, Jiang J. Simultaneous removal of SO_2 , NO and HgO through an integrative process utilizing a cost-effective complex oxidant. *J. Hazard. Mater*. **301** (2015): 74-83.
36. Bausach M, Pera-Titus M, Fite C, Cuill F, Izquierdo JF, Tejero J, Iborra M. Water-induced rearrangement of $Ca(OH)_2$ (0001) surfaces reacted with SO_2. *Aiche J*. **52** (2010): 2876-2886.
37. Sun Z, Wang S, Zhou Q, Hui SE. Experimental study on desulfurization efficiency and gas–liquid mass transfer in a new liquid-screen desulfurization system. *Appl. Energ*. **87** (2010): 1505-1512.
38. Gao J, Chen G, Fu X, Yin Y, Wu S, Qin Y. Enhancement mechanism of SO_2 removal with calcium hydroxide in the presence of NO_2. *Korean J. Chem. Eng*. **29** (2012): 263-269.
39. Li S, Li H, Wei L, Edding EG, Ren Q, Lu Q. Coal combustion emission and ash formation

characteristics at high oxygen concentration in a 1 MW th pilot-scale oxy-fuel circulating fluidized bed. *Appl. Energ*. **197** (2017): 203-211.

40. Chen L, Wang C, Zhao F, Zou C, Anthony EJ. The combined Effect of H_2O and SO_2 on the simultaneous calcination/sulfation reaction in CFBs. *Aiche J*. **65** (2019): 1256-1268.
41. Adewuyi YG, Sakyi NY, Arif KM. Simultaneous removal of NO and SO_2 from flue gas by combined heat and Fe^{2+} activated aqueous persulfate solutions. *Chemosphere*. **193** (2018): 1216-1225.
42. Liu D, Wall T, Stanger R. CO_2 quality control through scrubbing in oxy-fuel combustion: rate limitation due to S(IV) oxidation in sodium solutions in scrubbers and prior to waste disposal. *Int. J. Greenh. Gas Con*. **39** (2015): 148-157.
43. Torrente-Murciano L, White V, Petrocelli F, Chadwick D. Sour compression process for the removal of SO*x* and NO*x* from oxyfuel-derived CO_2. *Energy Procedia*. **4** (2011): 908-916.